DEVELOPMENT OF EQUIVALENT FORCE CONTROL METHOD FOR PSEUDO-DYNAMIC AND REAL-TIME SUBSTRUCTURE TESTS

Bin Wu[1], Guoshan Xu[1], Yan Li[2], Zhen Wang[1], Hongbin Jiang[1], P. Benson Shing[3], and Jinping Ou[1,4]

ABSTRACT

The equivalent force control (EFC) method replaces numerical iteration with a feedback control strategy to solve the nonlinear equations of motion in pseudodynamic and real-time substructure tests (RST) using an implicit integration method. The EFC method and its further development with an energy conserving integration method are presented in this paper. The effectiveness and accuracy of the EFC method are validated with quasi-static pseudo-dynamic tests of structures with buckling restrained braces and a reinforced concrete shear wall, and RST of structures with springs, buckling restrained braces, and an MR damper, respectively. It is shown that the EFC method can deliver excellent performance in all cases.

INTRODUCTION

In recent years, different approaches have been developed for real-time structural testing using servo-hydraulic actuators and reaction-wall or reaction-frame facilities. These include the effective force test method [Zhao *et al*. 2006] and real-time substructure test (RST) methods [Nakashima *et al*. 1992; Wu *et al*. 2005, 2006; Jung and Shing 2006]. The latter is a hybrid experimental technique that combines numerical simulation with physical testing. While the effective force method is conceptually simple and does not require real-time numerical computation during a test, it is not as versatile as RST methods.

While many different numerical algorithms are available for RST [Darby *et al*. 2001; Wu *et al*. 2005, 2006], for structures with multiple degree of freedom, an integration method with unconditional stability is highly desirable. Many implicit integration schemes are unconditionally stable but they require an iterative solution strategy for nonlinear systems, which is a challenge for RST. Implicit schemes have been implemented with different solution strategies to handle structural nonlinearity for RST, see, e.g., Shing *et al*. [2004], Bayer *et al*. [2005], Mosqueda and Ahmadizadeh [2007]. Bayer *et al*. [2005] and Jung and Shing [2006] have used an unconditionally stable implicit time integration method with a specially designed nonlinear solution strategy that combines a Newton-type iterative method with subincrementation. To avoid spurious loading and unloading of a specimen, the commands for the actuators are generated by a quadratic [Jung and Shing 2006] or linear [Bayer *et al*. 2005] interpolation based on iterative trial quantities.

[1] *School of Civil Engineering, Harbin Institute of Technology, Harbin, China*
[2] *School of Oil Gas Engineering, China University of Petroleum, Beijing, China*
[3] *Department of Structural Engineering, University of California, San Diego, CA, U.S.A.*
[4] *Dalian University of Technology, Dalian, China*

To avoid the numerical iteration process associated with implicit integration, Wu *et al*. [2007] have proposed the equivalent force control (EFC) method for RST. This paper describes basic concept of the EFC method, its further development with an energy conserving integration method, and applications to quasi-static pseudo-dynamic tests (PDT) and RST with various experimental substructures. These include buckling restrained braces (BRB), a reinforced concrete shear wall, elastic springs, and a Magnetorheological (MR) damper.

OVERVIEW OF EFC METHOD

EFC with Constant-Average-Acceleration Method

The concept of the EFC method can be explained by expressing the numerical solution of the equations of motion with the constant-average-acceleration (CAA) method in the following form [Wu *et al.* 2007]

$$\mathbf{R}_{\mathrm{N}}(\mathbf{d}_{i+1}) + \mathbf{K}_{\mathrm{PD}}\mathbf{d}_{i+1} + \mathbf{R}_{\mathrm{E}}(\mathbf{a}_{i+1}, \mathbf{v}_{i+1}, \mathbf{d}_{i+1}) = \mathbf{F}_{\mathrm{EQ},i+1} \tag{1}$$

where

$$\mathbf{K}_{\mathrm{PD}} = \frac{4\mathbf{M}_{\mathrm{N}}}{\Delta t^2} + \frac{2\mathbf{C}_{\mathrm{N}}}{\Delta t} \tag{2}$$

$$\mathbf{F}_{\mathrm{EQ},i+1} = \mathbf{F}_{i+1} + \mathbf{M}_{\mathrm{N}}\mathbf{a}_i + (\frac{4\mathbf{M}_{\mathrm{N}}}{\Delta t} + \mathbf{C}_{\mathrm{N}})\mathbf{v}_i + (\frac{4\mathbf{M}_{\mathrm{N}}}{\Delta t^2} + \frac{2\mathbf{C}_{\mathrm{N}}}{\Delta t})\mathbf{d}_i \tag{3}$$

In above equations, $\mathbf{d}$, $\mathbf{v}$, and $\mathbf{a}$ are the displacement, velocity, and acceleration vectors; $\mathbf{M}_{\mathrm{N}}$, $\mathbf{C}_{\mathrm{N}}$, $\mathbf{R}_{\mathrm{N}}$ are the mass, damping, and static restoring force vectors of the numerical substructure; $\mathbf{R}_{\mathrm{E}}$ is the restoring force vector of the experimental substructure including static, damping, and inertia forces; $\mathbf{F}$ is the external excitation force vector; and Δt the integration time interval; $\mathbf{K}_{\mathrm{PD}}$ is called the pseudo-dynamic stiffness, and $\mathbf{F}_{\mathrm{EQ}}$ the equivalent force (EF). The solution of Equation (1) can be interpreted as finding the response of a hybrid system, which consists of numerical and experimental substructures with real and pseudo-dynamic forces, to an explicit equivalent load. This response can be obtained by directly applying the equivalent force to the hybrid system, in which the numerical substructure and pseudo-dynamic forces are evaluated in a computer, using a force-feedback control strategy.

The block diagram representing an EFC system for a linear single-degree-of-freedom (SDOF) structure is shown in Fig. 1, in which K_{N} and K_{E} are the stiffness of the numerical and experimental substructures, respectively; C_{E} is the damping coefficient of the experimental substructure; and $T_{\mathrm{A}}(s)$ is the transfer function of the dynamics of the actuator-specimen system. The equivalent force controller shown in Fig. 1 is a proportional-integral-derivative (PID) controller, in which K_{P}, K_{I}, and K_{D} are the proportional, integral and derivative gains, respectively. The factor K_{F} after the equivalent force command $F_{\mathrm{EQ},i+1}$ is used to eliminate the steady-state error. After being processed by a force controller, the force error e_{EQ} between the equivalent force command modified by K_{F} and the equivalent force feedback $F'_{\mathrm{EQ},i+1}$ is converted to a displacement command d^{c}_{i+1} by a conversion factor C_{F}. Then, the actuator is controlled with a displacement control mode. The term d'_{i+1} represents the displacement response of the experimental substructure subjected to the command d^{c}_{i+1}. At the end of the (i+1)th step, the measured reaction force R_{E} and the calculated R_{N} is fed back to Equation (1) to calculate the displacement at this time step, and the corresponding velocity and acceleration responses of the structure are calculated according to the constant-average-acceleration method.

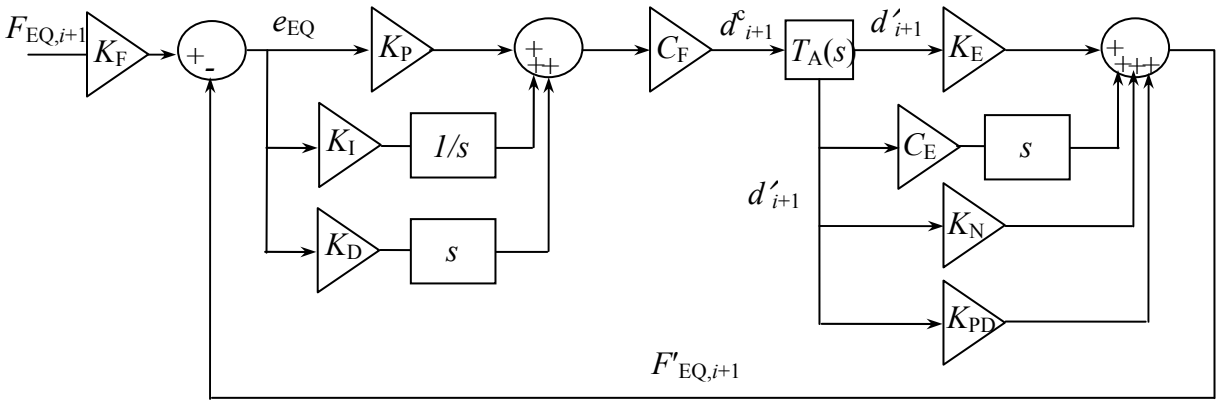

Fig. 1. Block diagram of EFC with PID controller for a SDOF structure.

EFC with Energy Conserving Method

It has been shown that the constant average acceleration method may not retain unconditional stability for certain nonlinear systems. To cope with this problem, Simo and Tarnow [1992] developed an energy conserving integration method, which retains unconditional stability for nonlinear systems. This method has been successfully used for RST with EFC [Li *et al.* 2007]. In this case, the solution scheme can be expressed as follows.

$$\mathbf{R}_{\mathrm{N}}(\mathbf{d}_{i+1}) + \mathbf{K}_{\mathrm{PD}}\mathbf{d}_{i+1} + \mathbf{R}_{\mathrm{EQ}}(\mathbf{d}_{i+1}) = \mathbf{F}_{\mathrm{EQ},i+1} \tag{4}$$

where

$$\mathbf{K}_{\mathrm{PD}} = \frac{2\mathbf{M}_{\mathrm{N}}}{\Delta t^2} + \frac{\mathbf{C}_{\mathrm{N}}}{\Delta t} \tag{6}$$

$$\mathbf{F}_{\mathrm{EQ},i+1} = \frac{\mathbf{F}_{i+1} + \mathbf{F}_i}{2} + \frac{2\mathbf{M}_{\mathrm{N}}}{\Delta t}\mathbf{v}_i + (\frac{2\mathbf{M}_{\mathrm{N}}}{\Delta t^2} + \frac{\mathbf{C}_{\mathrm{N}}}{\Delta t})\mathbf{d}_i \tag{7}$$

$\mathbf{R}_{\mathrm{EQ}}(\mathbf{d}_{i+1})$ is the equivalent restoring force, which can be calculated with

$$\mathbf{R}_{\mathrm{EQ}}(\mathbf{d}_{i+1}) = \frac{\Delta\mathbf{E}_{\mathrm{PE},i+1}}{\mathbf{R}_{\mathrm{E}}(\frac{\mathbf{d}_{i+1}+\mathbf{d}_i}{2})^{\mathrm{T}}\Delta\mathbf{d}_{i+1}}\mathbf{R}_{\mathrm{E}}(\frac{\mathbf{d}_{i+1}+\mathbf{d}_i}{2}) \tag{8}$$

in which $\Delta\mathbf{E}_{\mathrm{PE},i+1}$ is the increment of the energy stored or dissipated by the experimental substructure at step i+1, which is expressed as

$$\Delta\mathbf{E}_{\mathrm{PE},i+1} = \int_{\mathbf{d}_i}^{\mathbf{d}_{i+1}} \mathbf{R}_{\mathrm{E}}^{\mathrm{T}}(\mathbf{x})\mathrm{d}\mathbf{x} \tag{9}$$

Various numerical integration methods are available to evaluate the above expression; the rectangular rule was used in some of the tests presented in this paper.

DESIGN OF EF CONTROLLER

For simplicity, a linear SDOF structure with a negligible physical mass in the experimental substructure as shown in Fig.1 is used here to illustrate the design of EF controller. In Fig. 1, the force-displacement conversion factor C_F can be chosen to be

$$C_F = (K_N + K_{PD} + K_E)^{-1} \tag{10}$$

Based on Laplace's Terminal-Value Theorem[Ogata 2005], one can obtain the steady-state error of the whole system subjected to an EF input $F_{EQ,i+1}$. For the case of K_I=0, which means a P or PD controller is used, the steady-state error of the system subjected to a unit step EF command is $1/(1+K_P)$. Therefore, K_F should be equal to $(1+K_P)/K_P$ to eliminate the control error [Wu *et al.* 2007]. For the case of $K_I \neq 0$, which means a PI or PID controller is used, the corresponding steady-state error is zero, requiring that K_F be equal to 1.

EXPERIMENTAL VALIDATIONS

To verify the accuracy and effectiveness of the EFC method, both PDT and RST were conducted. The tests were performed at the Structural and Seismic Testing Center of Harbin Institute of Technology, in which a Flex Text GT controller was used to control a 2500 kN MTS actuator or a 250 kN Schenk actuator to impose displacement onto the specimen. The sampling frequency of the system was set to 2048 Hz.

Spring Specimen

The structural parameters of the SDOF spring structure as shown in Fig. 2 for RST were M_N=1.11×10^5 kg, K_N=2.19×10^6 N/m, and C_E=0. Two parallel linear springs as shown in Fig. 3 were used as the specimen. It should be noted that the configuration of the spring did not allow compressive loading. Therefore, the springs were preloaded in tension with a 14 mm extension at the neutral position, which means that the force output of the specimen is equal to the measured force minus the tensile force at the neutral position. The total measured stiffness of the two springs is 2.19×10^6 N/m, which was used to calculate the force-displacement conversion factor with Equation (10) in later tests. The integration time interval was chosen to be 0.02 s.

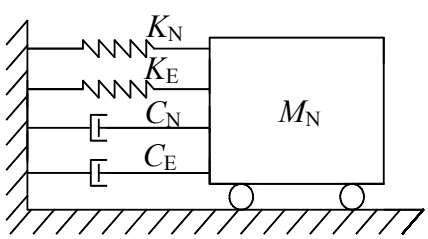

Fig. 2. Schematic of SDOF systems.

Fig. 3. Photograph of spring specimen in actual test.

The displacement response of the system from the RST with the Newmark average acceleration method for the El Centro (NS, 1940) earthquake ground motion record with a peak acceleration of 0.026 g is shown in Fig. 4. In this case, the initial displacement and velocity equal to zeros, the numerical damping ratio of the whole structure was 5%, and the EF controller parameters were K_P=0.2 and K_I=93.5/s. The result obtained from pure numerical simulation of the system response without an actuator model and with the central difference method (CDM) is also included in Fig. 4, which is considered as the true result here. The figure shows that the response of the EFC matches the pure numerical result obtained with the CDM very well. The EF response in Fig. 5 matches its command well at the end of each time step, which means that the result is accurate.

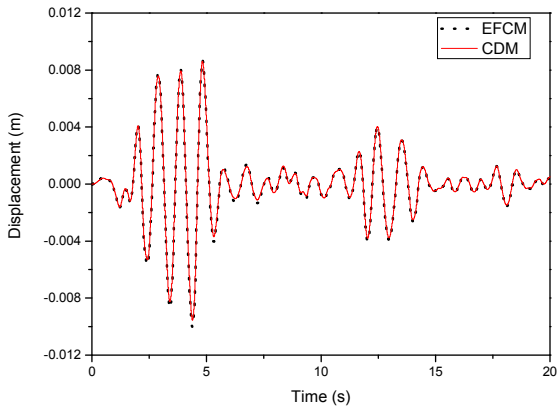

Fig. 4. Displacement responses to seismic input from RST of spring specimen.

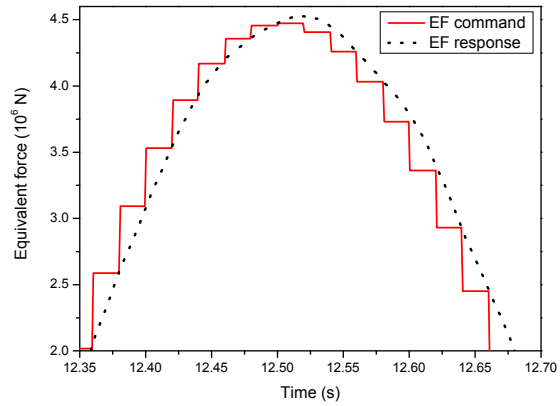

Fig. 5. Equivalent force response to seismic input from RST of spring specimen.

BRB Specimen

The schematic of the SDOF test structure with BRB specimen is shown in Fig. 6. Both the CAA and energy conserving methods were employed. The parameters of the numerical substructure are M_N=6×10^6 kg, K_N=1.2×10^8 N/m, and C_N=3.79×10^6 Ns/m. The integration time interval is 0.01s. The experimental substructures were two steel BRB. The length of the core plate of the braces was 1.18 m. The two braces differed from each other by their core plates as shown in Fig. 7. One had a flat core plate, and the other had a cruciform shape. The one with a flat core plate was used in PDT, and the other was used in RST. The steel plates were Grade Q235, whose Young's modulus was 2×10^5 MPa and nominal yield strength was 235 MPa. A photograph of the experimental setup is shown in Fig. 8.

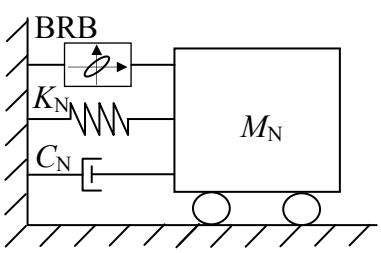

Fig. 6. Schematic of SDOF test structure with BRB specimen.

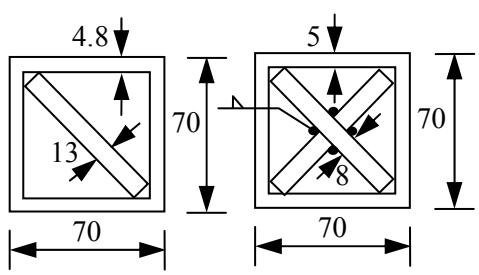

Fig. 7. Cross sections of BRB for test.

Fig. 8. Photograph of experimental setup with BRB specimen.

PDT. The calculated elastic stiffness of the BRB for the PDT was 1.4×10^8 N/m, and the damping ratio provided by the numerical substructure was 4.8%. For the PDT with EFC, the equivalent force commands were generated by linear interpolation with five sub-commands for each time integration step. The initial stiffness and secant stiffness at the previous integration time step of the BRB specimen were used to calculate the force-displacement conversion factor. The initial displacement and velocity equal to zeros. The excitation was chosen to be the El Centro (NS, 1940) ground motion with a peak acceleration of 0.3 m/s^2. The EF controller parameter was K_P=0.05. The loading rate was 25 times slower than the real time. For comparison, the result from CDM is considered as the true result. The displacement responses and the corresponding hysteretic loops from the test are shown in Fig. 9. In Fig.9a, one can see

that these four responses match that obtained with the CDM very well. This should be expected by considering that the initial stiffness of the BRB is very small as compared to the pseudo-dynamic stiffness of the hybrid system as discussed in Wu *et al*. [2008].

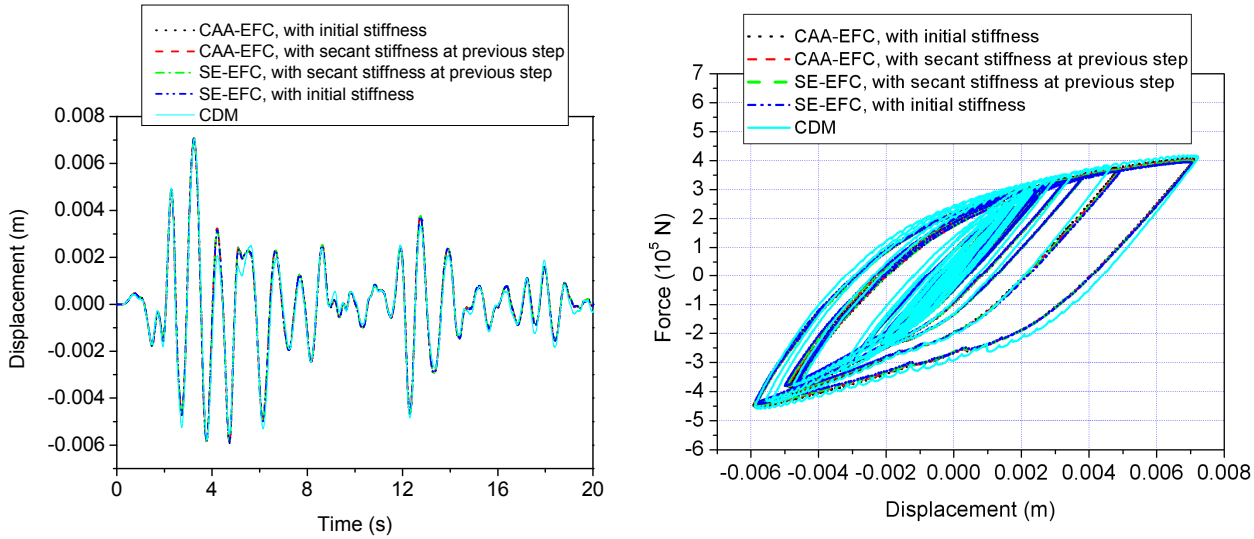

(a) Displacement responses (b) Hysteretic loops

Fig. 9 Displacement responses from PDT and the corresponding hysteretic loops of BRB.

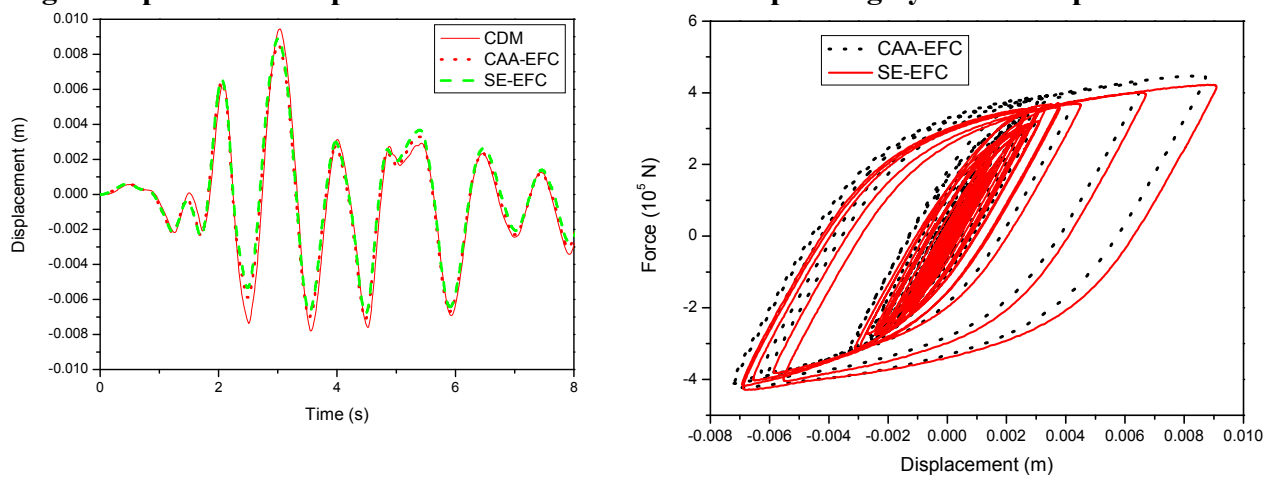

(a) Displacement responses (b) Hysteretic loops

Fig. 10 Displacement responses from RST and the corresponding hysteretic loops of BRB.

RST. In RST, the calculated initial stiffness of the brace was 1.5×10^8 N/m, slightly greater than that used in the PDT. A modified version of the third order polynomial extrapolation method was used to compensate for the delay [Li 2007]. The secant stiffness of the BRB specimen at the previous integration time step was used to calculate the force-displacement conversion factor. The excitation used was again the El Centro (NS, 1940) ground motion but with a peak acceleration of 0.4 m/s^2. For comparison, the result from CDM is considered as the true result. The displacement responses and the corresponding hysteretic loops from the test are shown in Fig. 10. Fig.10a shows that the two responses agree well with that obtained with the CDM.

MR Damper Specimen

To suppress the vibration mainly induced by ice and earthquake loads, an isolation layer was designed between the main deck and top of the supporting jacket of the JZ20-2NW offshore platform located in Bohai Gulf of China. The photo of the platform is shown in Fig. 11. The detail of the isolation layer is shown in Fig. 12. It was composed of 8 rubber isolators and 8 MR dampers. The isolators were placed at the four corners and the center area of the isolation layer. The dampers were incorporated around the corners of the isolation layer. The platform model was simplified into an eight-degrees-of-freedom (8DOF) model as shown in Fig. 13. The structural parameters except for MR dampers can be found in Wu *et al*. [2008].

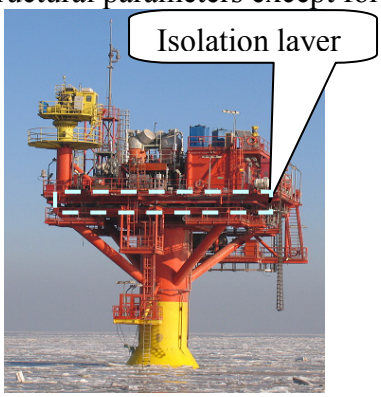

Fig. 11. Photo of JZ20-2NW offshore platform.

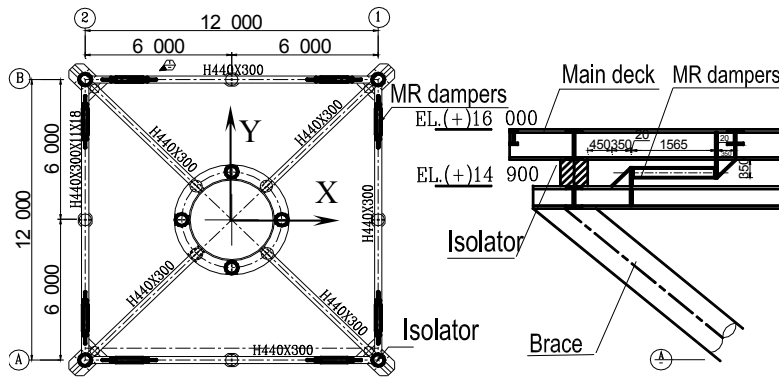

Fig. 12. Isolation layer of JZ20-2NW platform.

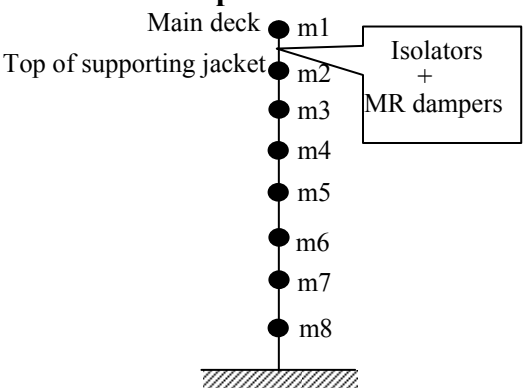

Fig. 13. 8DOF model of the JZ20-2NW offshore platform.

Fig. 14. Photograph of experimental setup with MR specimen.

For comparison, both the CAA-EFC and the CDM with conventional displacement control were used for the RSTs. The MR damper with zero drive voltage acting as a passive fluid viscous damper was the experimental substructure and the remainder of the structure was the numerical substructure. The test setup is shown in Fig. 14. The equivalent force command calculated with Equation (3) in each integration time step was divided into 20 sub-steps using linear interpolation in order to smooth the velocity response. The earthquake inputs were the El Centro (NS, 1940) and Taft (N21E, 1952) with peak acceleration of 1.00 m/s^2, and Tianjin (1976) with peak acceleration of 0.35 m/s^2. The control gain of the equivalent force controller was K_P=0.5. The integration time interval in the tests was chosen to be 0.02 s.

The experimental drifts of the isolation layer subjected to El Centro (NS, 1940) earthquake are shown in Fig. 15. It is seen that the RST response with the CDM diverges, while that with the EFC method remains stable. The pure numerical result without dampers is also shown in Fig. 15, where the significant control effect of the dampers is observed. Fig. 16 shows hysteretic loops of the MR damper. Similar conclusions can be obtained from the tests of Taft (N21E, 1952) and Tianjin (1976) earthquake records.

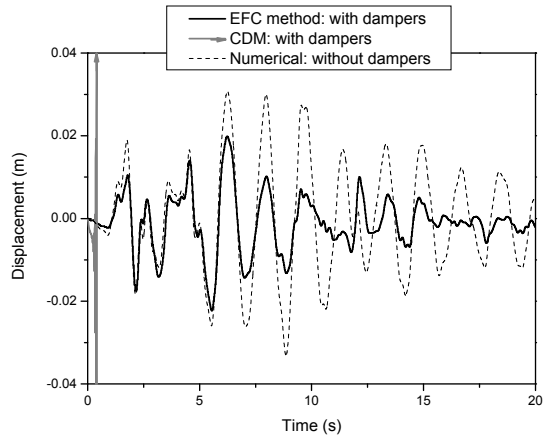

Fig. 15. Drifts of the isolation layer.

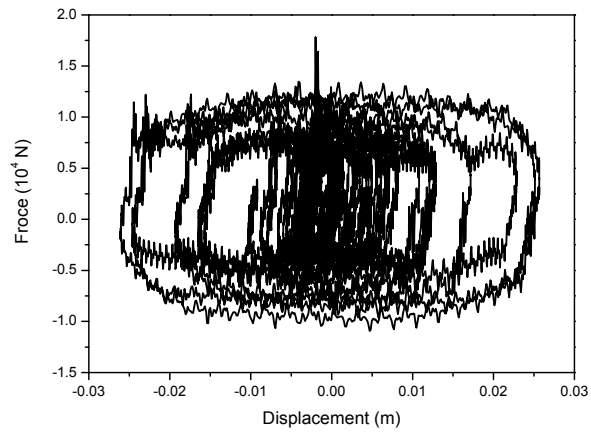

Fig. 16. Hysteretic loops of MR damper.

RC Shear Wall Specimen

The PDT of the SDOF structure as shown in Fig. 6 with a RC shear wall specimen was conducted with CAA-EFC. The structural parameters are M_N=9.43×10^5 kg, K_N=1.019×10^7 N/m, and C_N=5.922×10^5 Ns/m. The precast RC shear wall was designed with a novel method for in situ connection of precast walls [Zhang 2009]. The corresponding test setup is shown in Fig. 17. The parameters of the specimen are listed in Tab. 1. More information about this specimen can be found in Zhang [2009]. The initial stiffness of the specimen obtained with preliminary quasi-static test is 2.7×10^7 N/m. The circular frequency and damping ratio of the structure are 6.28 rad/s and 5%, respectively. The integration time interval is 0.01s.

Table 1. Parameters of the precast RC shear wall specimen

Strength grade of steel bar	Strength grade of Concrete	Size of Specimen (mm×mm×mm)	Longitudinal Bar	Stirrup
HRB335	C30	2200×1400×200	12@200	8@200

The displacement responses of the structure subjected to El Centro (NS, 1940) ground motion with a peak acceleration of 0.5 m/s^2 are shown in Fig. 18. The EF controller gains are K_P=0.5 and K_I=10/s. Fig. 18 shows that the response of the actuator tracks its command well and the displacement response of the specimen matches closely with that of the structure. The obvious difference is also observed between displacement responses of the actuator and the specimen. The difference may be attributed to the slippage between the specimen and the strong floor to which it is attached. It is indicated from the good match of the responses of the specimen and the structure that the result from the EFC is reliable and the EFC method can effectively compensate for the specimen slippage if it is not fastened firmly enough to the floor. Fig. 19 shows the hysteretic loops of the specimen. The thin hysteretic loops imply its poor energy dissipation capacity after severe damages in the quasi-static cyclic test with large deformation prior to this

PDT. The agreement of EF command and response depicted in Fig. 20 also shows the accuracy of the test result.

Fig. 17. Test setup for RC shear wall specimen.

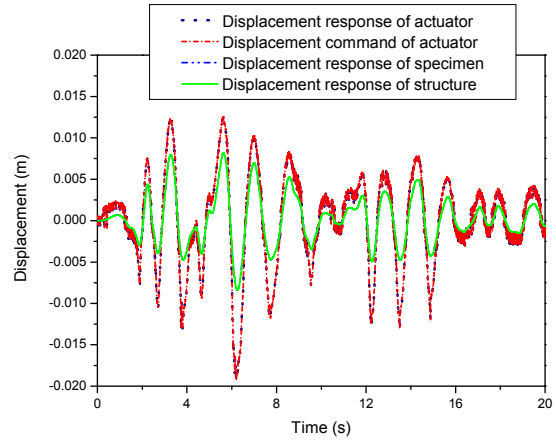

Fig. 18. Comparisons of displacement histories.

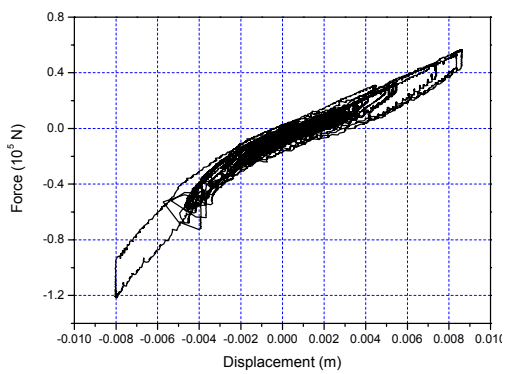

Fig. 19. Hysteretic loops of the specimen.

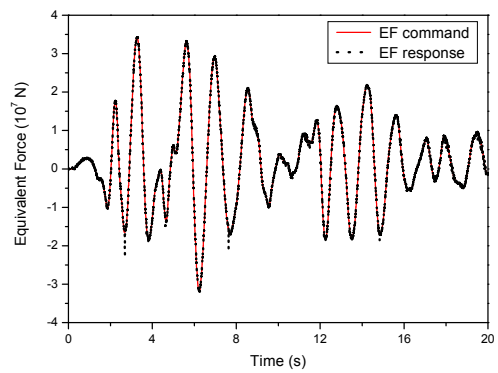

Fig. 20. EF Command and response.

CONCLUSIONS

The basic idea of EFC for hybrid simulation and its further development with energy-conserving integration method are reviewed in this paper. The effectiveness and accuracy of the method were validated with PDT of structures with buckling restrained braces and reinforced concrete shear wall specimen, and RST of structures with springs, buckling restrained braces, and MR damper specimen. It is shown that the EFC method can deliver excellent performance for both RST and PDT of structures, even when large slippage exists between the specimen and attaching floor.

ACKNOWLEDGEMENTS

This work was supported by Grant 90715036 from the National Science Foundation of China, and Grant 2008419073 from China Earthquake Ministration. The assistance of Mr. Yunfei Ma and Mr. Darui Zhou of the Structural and Seismic Testing Center, Harbin Institute of Technology, with the operation of the MTS testing system is gratefully acknowledged.

REFERENCES

Bayer, V., Dorka, U. E., Füllekrug, U., and Gschwilm, J. 2005. On real-time pseudo-dynamic sub-structure testing: algorithm, numerical and experimental results. *Aerospace Science and Technology* 9:223–232.

Darby, A. P., Blakeborough, A., and Williams, M. S. 2001. Improved control algorithm for real-time substructure testing. *Earthquake Engineering & Structural Dynamics* 30:431–448.

Jung, R. Y., and Shing, P. B. 2006. Performance evaluation of a real-time pseudodynamic test system. *Earthquake Engineering and Structural Dynamics* 35:789–810.

Li, Y. 2007. *Seismic performance of buckling-restrained braces and substructure testing methods*. Doctoral Thesis, Harbin Institute of Technology (in Chinese).

Mosqueda, G., and Ahmadizadeh, M. 2007. Combined implicit or explicit integration steps for hybrid simulation. *Earthquake Engineering & Structural Dynamics* 36: 2325–2343.

Nakashima, M., Kato, H., and Takaoka, E. 1992. Development of real-time pseudo dynamic testing. *Earthquake Engineering & Structural Dynamics* 21:79–92.

Ogata, K. 2005. *Modern Control Engineering*. Prentice-Hall (Reprinted by Tsinghua University Press, Beijing).

Shing, P. B., Wei, Z., Jung, R. Y., and Stauffer, E. 2004. Nees fast hybrid test system at the University of Colorado. *Proceedings of the 13th World Conference on Earthquake Engineering*. Vancouver, B.C., Canada, paper No. 3497.

Simo, J. C., Tarnow, N. 1992. The Discrete Energy-Momentum Methods: Conserving Algorithms for Nonlinear Elastodynamics. *Zeitschrift für Angewandte Mathematik und Physik* (ZAMP) 43:757–793.

Wu, B., Bao, H., Ou, J., and Tian, S. 2005. Stability and accuracy analysis of central difference method for real-time substructure testing. *Earthquake Engineering & Structural Dynamics* 34:705–718.

Wu, B., Xu, G. S., Wang, Q. Y., and Williams, M. 2006. Operator-splitting method for real-time substructure testing. *Earthquake Engineering & Structural Dynamics* 35:293–314.

Wu, B., Wang, Q. Y., Shing, P. B., and Ou, J. P. 2007. Equivalent force control method for generalized real-time substructure testing with implicit integration. *Earthquake Engineering & Structural Dynamics* 36:1127–1149.

Wu, B., Xu, G. S., Li, Y., Shing, P. B., and Ou, J. P. 2008. Performance and application of equivalent force control method for real-time substructure testing. Submitted to *Journal of Engineering Mechanics* (ASCE).

Zhang H. S. 2009. *Experimental study on lap-joint of steel bar of precast concrete shear walls*. Master's Thesis, Harbin Institute of Technology. (in Chinese)

Zhao, J., French, C., Shield, C., and Posbergh, T. 2006. Comparison of tests of a nonlinear structure using a shake table and the EFT method. *Journal of Structural Engineering* 132(9):1473–1481.